Effect of $NaNbO_3$ substitution on the quantum paraelectric behavior of $CaTiO_3$

Saurabh Tripathi,[1] Anil Kumar,[2] Umesh V. Waghmare,[2] and Dhananjai Pandey[1]
[1]*School of Materials Science and Technology, Banaras Hindu University, Varanasi 221005, India*
[2]*Theoretical Sciences Unit, Jawaharlal Nehru Centre for Advanced Scientific Research, Bangalore 560064, India*
(Received 15 April 2010; revised manuscript received 4 May 2010; published 1 June 2010)

Low-temperature dielectric and x-ray diffraction studies on $NaNbO_3$ substituted $CaTiO_3$ reveals suppression of quantum fluctuations, when the concentration of $NaNbO_3$ exceeds 2%. Group-subgroup considerations in conjunction with the knowledge of unstable phonon modes, obtained by first-principles calculations, show that the low-temperature phase is a unique type of ferrielectric phase that exhibits planar antiferroelectric and axial ferroelectric orders.

DOI: 10.1103/PhysRevB.81.212101 PACS number(s): 77.80.−e, 77.84.Cg, 77.84.Ek

Ferroelectric and antiferroelectric phase transitions involve softening and freezing of optical phonons corresponding to the Brillouin-zone center and zone boundary.[1] Usually in all these transitions, the energy balance between the polar or antipolar dipolar ordering energy and the thermal fluctuations stabilizes the low-temperature phase. However, when the transition temperatures are rather low, the ordering energy competes with the zero-point vibrational energy (quantum fluctuations) of the lattice.[2] In quantum paraelectrics such as $SrTiO_3$,[3] $KTaO_3$,[4] and $CaTiO_3$ (CT),[5] quantum fluctuations are believed to stabilize the paraelectric state leading to the saturation of the ferroelectric soft-mode frequency[6] and the dielectric permittivity[3] at very low temperatures. The temperature variation of the dielectric permittivity in such quantum paraelectrics is found to follow the quantum-mechanical mean-field formula originally due to Barrett,[7] $\varepsilon' \approx M/[(T_1/2)\coth(T_1/2T)-T_c]$, which in the limit of $T \gg T_1$ reduces to the classical Curie-Weiss law.

It is possible to suppress quantum fluctuations by controlling the energy balance between quantum fluctuations and dipolar orderings through cationic substitutions creating random site ionic dipoles,[8] external pressure,[9] electric field,[6,10] and isotope exchange method, i.e., replacing ^{16}O with a larger mass ^{18}O.[11] The suppression of quantum fluctuations and stabilization of the low-temperature ferroelectric and antiferroelectric phases is usually evidenced by the observation of an anomaly at the phase-transition temperature in dielectric constant, specific heat, and crystallographic parameters, etc. $SrTiO_3$ and $KTaO_3$ are prototypical paradigms of quantum paraelectrics where cationic substitution induced ferroelectric and dipole glass transitions have been investigated extensively.[8,12] These materials are characterized by a positive Curie-Weiss temperature in their quantum paraelectric state. In contrast no systematic study on the role of chemical substitutions in CT with negative Curie-Weiss temperature exists, barring an exploratory investigation.[13] Further, we do not understand the origin of negative Curie-Weiss temperature in $CaTiO_3$, nor do we understand the nature of incipient instability leading to quantum paraelectric behavior in this material.

We present here the results of a systematic dielectric and x-ray diffraction (XRD) study in conjunction with the results of first-principles calculations of the phonon dispersion on the mixed system $(1-x)CaTiO_3$-$xNaNbO_3$ (CT-xNN) for $0 \leq x \leq 0.30$. This system was chosen with a view that the replacement of Ti^{4+} with much heavier Nb^{5+} should reduce the zero-point vibrational energy and hence facilitate the stabilization of the low-temperature phase. The Na^+ substitution at the Ca^{2+} site ensures local level charge compensation. Our *ab initio* first-principles calculations reveal that the rotational instabilities corresponding to $M(q=1/2,1/2,0)$ and $R(1/2,1/2,1/2)$ points and the polar instability at the zone center $\Gamma(q=0,0,0)$ of the optical branch of the phonon spectrum of $CaTiO_3$ (Ref. 14) persist even in the cubic paraelectric phase of the mixed CT-xNN system. The dielectric studies on the mixed system reveal suppression of quantum fluctuations as evidenced by the appearance of a peak in the temperature dependence of the dielectric permittivity for $0.02 \leq x \leq 0.30$. Low-temperature XRD studies reveal anomalies in the unit-cell parameters around the dielectric peak temperature. Symmetry considerations in conjunction with the knowledge of unstable modes from first-principles calculations and the Rietveld analysis of the powder XRD data reveal that the low-temperature phase exhibits planar antiferroelectric order, which is responsible for the negative Curie-Weiss temperature, and axial ferroelectric ordering of dipoles. Such crystals that exhibit antiferroelectric order along one axis and ferroelectric order along another axis have been termed as ferrielectric in the literature.[15]

CT-xNN samples were prepared by solid-state route, the details of which are described elsewhere.[16] The XRD data were collected on a Rigaku 18 kW rotating anode based powder diffractometer using Cu $K\alpha$ radiation, whose details are given in Ref. 16. Rietveld and Le-Bail analyses of the powder x-ray diffraction data were carried out using the "FULLPROF" package.[17] Our total-energy calculations are based on the ABINIT (Ref. 18) implementation of density-functional theory with an exchange-correlation energy within a local-density approximation. It involves solving the Kohn-Sham equations by a fixed-potential-based iterative conjugate-gradient minimization of one-electron energies in the ground state and iteratively achieves the self-consistency of the Kohn-Sham potential. The potential of the nucleus and the core electrons was approximated with norm-conserving pseudopotentials. We use $6\times6\times6$ Monkhorst-Pack mesh for the sampling of the Brillouin zone of the cubic structure, and an energy cutoff of 40 hartree (1 hartree is equal to 27.211 eV) on the plane-wave basis to represent Kohn-Sham wave functions. Ionic relaxation was performed using a

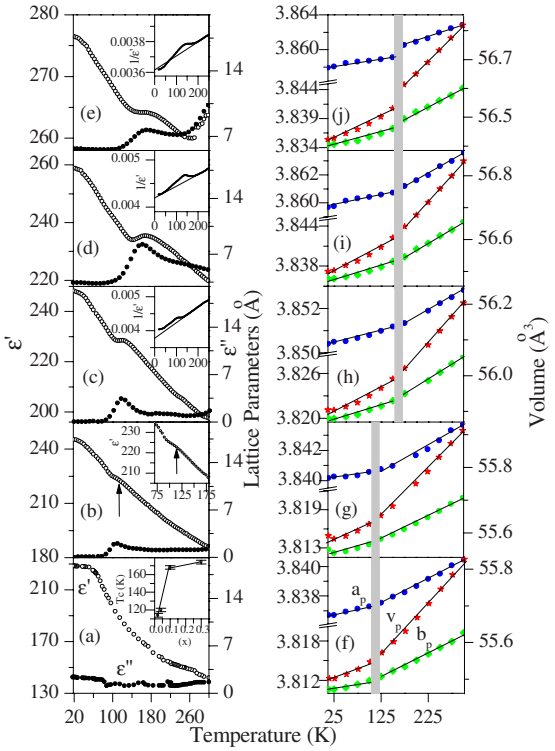

FIG. 1. (Color online) The left side panel depicts the real (ε') and imaginary (ε'') parts of the dielectric constant of CT-xNN with temperature: (a) x=0, (b) x=0.02, (c) x=0.04, (d) x=0.10, and (e) x=0.30. The open and filled circles correspond to ε' and ε'', respectively. The inset in (a) depicts the variation of ε' peak temperature (T_c) with (x). Insets in (c), (d), and (e) depict Curie-Weiss fits for $1/\varepsilon'$ versus T plot. The inset in (b) gives a magnified view of the weak dielectric anomaly at the phase-transition temperature. The right-hand panel depicts the evolution of the equivalent orthorhombic cell parameters (a_p,b_p) and volume (v_p) with temperature: (f) x=0.02, (g) x=0.04, (h) x=0.10, and (i) x=0.30 using *Pnma* space group. (j) depicts the cell parameter anomalies using $Pmn2_1$ space group below and *Pnma* above the phase-transition temperature for x=0.30. The transition temperature lies in the shaded region in the right-hand panel.

Broyden-Fletcher-Goldfarb-Shanno-based technique to minimize energy. We use virtual-crystal approximation (VCA) method to study the solid solution of CT-xNN in the cubic perovskite structure. We prefer to use VCA compared to supercell method to model the solid solution because it has already been shown[19] that VCA is good enough to describe the properties of perovskite alloys, whereas supercell method requires a large supercell to mimic the properties of solid solutions and alloys, and hence is computationally very demanding. However, to see any unknown fictitious behavior of VCA, we also use supercell method to calculate phonon frequencies of CT-0.25NN and found that VCA frequencies are consistent with the cubic symmetry, whereas the supercell method gives anomalous splitting of degenerate modes as it breaks the directional symmetry due to doping.

Figure 1 (left panels) depicts the variation of the real $\varepsilon'(T)$ and imaginary $\varepsilon''(T)$ parts of the dielectric permittivity of CT-xNN with temperature at a measuring frequency of 10 kHz. For pure CT [see Fig. 1(a)], ε' increases with decreasing temperature up to ~60 K below which it exhibits saturation, characteristic of a quantum paraelectric, in agreement with an earlier report.[5] On doping CT with 2%NN (CT-0.02NN), the $\varepsilon'(T)$ and $\varepsilon''(T)$ plots show the appearance of a weak anomaly around 114 K. This anomaly is better revealed in the $\varepsilon''(T)$ plot and the zoomed part of $\varepsilon'(T)$ shown in the inset of Fig. 1(b). This suggests that the quantum fluctuations of the lattice in CT are suppressed by ~2%NN substitution leading to a phase transition with a $T_c \sim 114$ K. On increasing the NN content, the phase-transition temperature shifts to higher side as can be seen from Figs. 1(c)–1(e) for CT-xNN compositions with x=0.04, 0.10, and 0.30. The Curie-Weiss fits, shown in the insets to Figs. 1(c)–1(e) for $\varepsilon'(T)$ for $T > T_c$, reveal negative T_c, which is a characteristic of an antiferroelectric or ferrielectric transition.[20] For a ferroelectric transition, the Curie-Weiss temperature cannot be negative and hence the dielectric anomalies shown in Figs. 1(b)–1(e) are not due to a ferroelectric transition. The variation of the phase-transition temperature (T_c) with composition (x) is depicted in the inset of Fig. 1(a).

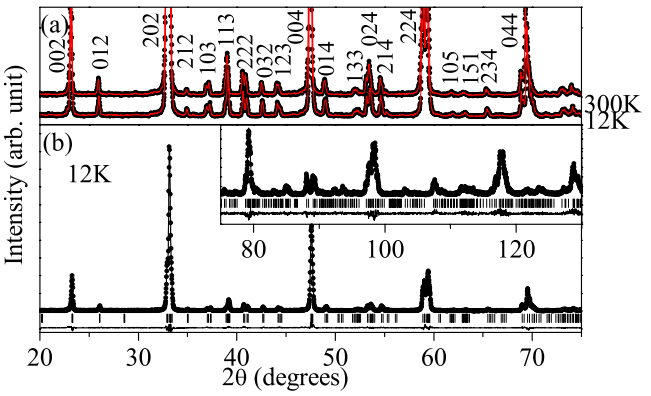

FIG. 2. (Color online) (a) Evolution of powder x-ray diffraction pattern of CT-0.10NN with temperature. The Miller indices are with respect to a doubled perovskite cell. (b) Observed (dots), calculated (continuous line), and difference (bottom line) profiles obtained after Rietveld analysis of powder x-ray diffraction data for CT-0.10NN at 12 K using orthorhombic space group $Pmn2_1$.

Antiferroelectric or ferrielectric phase transitions in perovskites lead to the doubling or multipling of the primitive unit cell leading to the appearance of characteristic superlattice reflections in the diffraction profiles. The XRD pattern taken at 300 K shown in Fig. 2(a) already contains superlattice reflections, with Miller indices represented by three odd (ooo), two odd and one even (oeo), and one odd and two even (eoe) integers (e.g., 113, 123, and 212 in the figure) with respect to a doubled pseudocubic cell, which arise, respectively, due to antiphase octahedral tilts, in-phase octahedral tilts, and antiparallel cationic (Ca^{2+}/Na^{1+}) displacements[21] in the paraelectric orthorhombic phase. However, we do not observe appearance of additional superlattice reflections below the phase-transition temperature as can be seen from a comparison of the XRD patterns of CT-0.10NN at 300 and 12 K shown in Fig. 2(a). The nonappearance of any new superlattice reflection in the antiferroelectric or ferrielectric phase of CT-xNN is not surprising since the structure of the paraelectric phase already

corresponds to a multipled cell with cell dimensions of $\sqrt{2}a_p \times 2b_p \times \sqrt{2}c_p$, in the *Pnma* space group, where a_p, b_p, and c_p are the elementary perovskite cell parameters. It is therefore expected that the atoms within this already multipled cell undergo antiparallel displacements without causing the appearance of any new superlattice peak. Such a rearrangement of atoms within the unit cell should manifest through anomalies in the crystallographic unit-cell parameters. This indeed is observed as can be seen from Figs. 1(f)–1(i) which depict the orthorhombic cell parameters obtained by Rietveld refinement using *Pnma* space group. Given that the XRD measurements were carried out at 25 K interval, the temperatures corresponding to the anomalies in the unit-cell parameters are found to be in reasonable agreement with the temperatures at which the peaks in $\varepsilon'(T)$ and $\varepsilon''(T)$ are seen in Figs. 1(b)–1(e). This clearly indicates that the structural changes accompany the antiferroelectric or ferrielectric transition.

In order to arrive at the correct space group of the low-temperature phase and hence the nature of dipolar ordering, we have used symmetry arguments using the ISOTROPY package.[22] To use this, we need to know the various unstable phonon modes in the cubic phase of CT-*x*NN which on freezing give the room-temperature orthorhombic *Pnma* phase and the low-temperature antiferroelectric or ferrielectric phase successively. For pure CT, first-principles calculations carried out by Cockayne and Burton[14] revealed that Γ_{15}, M_3, M_5', and R_{25} modes corresponding to the $\Gamma(q=0,0,0)$, $M(q=1/2,1/2,0)$, $R(q=1/2,1/2,1/2)$, and $X(q=1/2,0,0)$ points of the cubic Brillouin zone are unstable. The M_3 and R_{25} unstable modes representing rotational instabilities in the cubic phase of CT lead to the room-temperature orthorhombic phase of CT in the *Pnma* space group with $a^-b^+a^-$ tilt system in Glazer's notation.[21] In addition to M_3 and R_{25}, the M_5' and Γ_{15} modes are also unstable in the cubic phase of CT, which could have frozen at low temperatures but for the competition from the quantum fluctuations. In order to understand as to what happens to these unstable modes in CT-*x*NN, we have carried out first-principles calculation of phonons of CT and CT-0.25NN, with the latter being under VCA. We compare in Table I of the supplementary material[23] the unstable phonon modes of CT as reported by Cockayne and Burton and those obtained by us for CT and CT-0.25NN, respectively. Our results on CT are in broad agreement with those reported by Cockayne and Burton. Further, our calculations show that even after 25%NN substitution, the Γ_{15}, M_3, and R_{25} modes are still unstable with imaginary frequencies. The complete phonon dispersion curves of cubic CT and CT-0.25NN are displayed in Fig. 3. Here, the imaginary frequency domain of the curve plotted on the negative frequency axis corresponds to the unstable modes. The hardening of these modes leads to the low-symmetry structure which may be a maximal subgroup of the parent phase for a second-order phase transition as per Landau criterion. Now, since the combination of zone-boundary and zone-center optical phonon modes is known to lead to antiparallel arrangement of dipoles, which may be responsible for the negative Curie-Weiss temperature, we considered combinations of the Γ_{15}, M_3, and R_{25} irreps (here, irreps stands for irreducible representations[22] of the $Pm\bar{3}m$ space group) in the cubic phase to predict the possible space groups of the low-temperature phase. We imposed the restriction that the space group of the low-temperature phase should be a subgroup of *Pnma* space group of the paraelectric phase. We also put the restriction that the unit-cell size $(\sqrt{2}a_p \times 2c_p \times \sqrt{2}b_p)$ of the paraelectric phase is retained in the low-temperature phase, as our XRD results reveal that the cell size does not change in the low-temperature phase. Using the ISOTROPY package[22] we find that the static displacements due to frozen distortion modes R_{25} and M_3 of the high-symmetry cubic structure $Pm\bar{3}m$ lead to *Pnma* space group for the paraelectric phase, whereas the displacements due to the combination of R_{25} and M_3 with polar zone-center mode Γ_{15} lead to $Pmc2_1$, $Pmn2_1$, and $Pna2_1$ space groups for the low-temperature antiferroelectric or ferrielectric phase.

TABLE I. Refined structural parameters of the ferrielectric phase of NN-0.10CT at 12 K using the orthorhombic space group $Pmn2_1$.

Atoms	*X*	*Y*	*Z*	*B* (Å^2)
Na_1/Ca_1	0.000	0.713(1)	0.020(3)	0.2(2)
Na_2/Ca_2	0.000	0.214(1)	0.509(3)	0.2(2)
Nb/Ti	0.250(1)	0.249(1)	0.006(2)	0.26(3)
O_1	0.000	0.261(2)	0.956(4)	0.1(2)
O_2	0.000	0.776(3)	0.610(4)	0.1(3)
O_3	0.282(1)	0.552(2)	0.813(1)	0.5(3)
O_4	0.795(1)	0.969(2)	0.233(1)	0.1(2)

A_0=7.6349(4) Å, B_0=5.4411(3) Å, C_0=5.3727(3) Å, R_p=7.88, R_{WP}=11.6, R_{exp}=9.14, R_B=4.55, χ^2=1.61.

Having arrived at three plausible space groups for the low-temperature phase of CT-*x*NN, we carried out Rietveld refinements for each of them using the 12 K XRD data, as also for the room-temperature *Pnma* space group. R_{WP}'s for $Pmn2_1$, $Pmc2_1$, $Pna2_1$, and *Pnma* space groups are 11.6, 13.0, 12.7, and 12.3, respectively. Thus, the $Pmn2_1$ space group gives the lowest R_{WP} and χ^2 and should therefore be

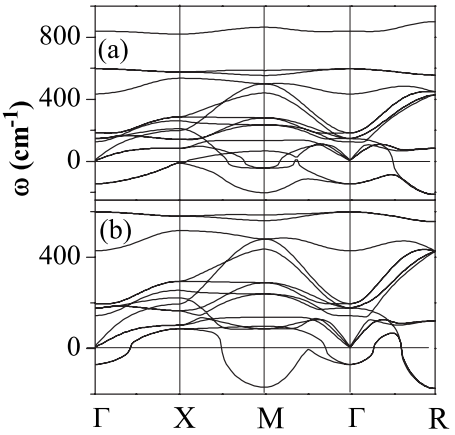

FIG. 3. Phonon dispersion curves for cubic CT and CT-0.25NN.

the correct space group for the low-temperature phase. Durbin-Watson statistics[24,25] also favors this space group. The Rietveld fit for this space group is depicted in Fig. 2(b), while the refined structural parameters are given in Table I. The parameters R_P, R_{WP}, R_{exp}, and R_B are various measures of agreement between observed and calculated intensities, as defined in Ref. 25. The variation of the equivalent elementary perovskite unit-cell parameters of CT-0.30NN obtained by Rietveld refinement using $Pmn2_1$ and $Pnma$ space groups below and above the phase-transition temperature (T_c) is shown in Fig. 1(j). The discontinuous change in the unit-cell volume at the transition temperature reveals the weakly first-order character of the phase transition in CT-xNN.

The $Pmn2_1$ space group is a noncentrosymmetric space group. For an antiferroelectric phase, the requirement of antiparallel sublattice polarization leads to a centrosymmetric space group. Thus, the observed structural data and the symmetry analysis of the phase transition are not consistent with simple antiferroelectric phase transition. We have already ruled out the possibility of ferroelectric phase transition because of negative T_c. This leaves only one possibility, i.e., of ferrielectric transition which also leads to negative Curie-Weiss temperature.[20]

Analysis of the ionic displacements in the $Pmn2_1$ space group of the low-temperature phase of CT-0.10NN given in Table I reveals that the direction (which is [010]) and magnitude of the net polarization in the XY planes at $z=0,1/4$ are equal and opposite to that in the planes at $z=1/2$ and 3/4, respectively, revealing antiferroelectric coupling (see Fig I of the supplementary material for an schematic representation of the displacement directions).[23] In addition to this planar antiferroelectric order, there is also a Z component of ionic displacements which gives net ferroelectric polarization in the [001] direction. We have calculated the polarization using nominal valence and atomic displacement using the formula $P=\Sigma_i(\Delta z_i Q_i e)/V$, where Δz_i is the atomic displacement along the c axis from the corresponding position in the orthorhombic structure, $Q_i e$ is the ionic charge of the ith constituent ion, and V is the unit-cell volume. Using our Rietveld refined positional coordinates, the net ionic polarization comes out to be 16.19 $\mu C/cm^2$ along [001] under point charge approximation. Thus, $NaNbO_3$ substitution not only suppresses the quantum fluctuations of $CaTiO_3$ but also stabilizes a unique type of ferrielectric phase exhibiting planar antiferroelectric and axial ferroelectric orders. This ferrielectric phase can be visualized to have resulted from the displacements associated with the freezing of the polar Γ_{15} and rotational R_{25} and M_3 unstable modes of the paraelectric cubic phase of CT-xNN.

[1] R. Blinc and B. Zeks, *Soft Modes in Ferroelectrics and Antiferroelectrics* (North Holland Publishing Co., Amsterdam, 1974).
[2] U. T. Höchli, Ferroelectrics **35**, 17 (1981).
[3] K. A. Müller and H. Burkard, Phys. Rev. B **19**, 3593 (1979).
[4] B. E. Vugmeister and M. D. Glinchuk, Rev. Mod. Phys. **62**, 993 (1990).
[5] I. S. Kim, M. Itoh, and T. Nakamura, J. Solid State Chem. **101**, 77 (1992).
[6] P. A. Fleury and J. M. Worlock, Phys. Rev. Lett. **18**, 665 (1967).
[7] J. H. Barrett, Phys. Rev. **86**, 118 (1952).
[8] J. G. Bednorz and K. A. Müller, Phys. Rev. Lett. **52**, 2289 (1984); V. V. Lemanov, E. P. Smirnova, and E. A. Tarakanov, Phys. Solid State **39**, 628 (1997).
[9] H. Uwe and T. Sakudo, Phys. Rev. B **13**, 271 (1976); J. Phys. Soc. Jpn. **23**, 546 (1967).
[10] P. A. Fleury, J. F. Scott, and J. M. Worlock, Phys. Rev. Lett. **21**, 16 (1968); J. M. Worlock and P. A. Fleury, *ibid.* **19**, 1176 (1967).
[11] M. Takesada, M. Itoh, and T. Yagi, Phys. Rev. Lett. **96**, 227602 (2006); M. Itoh, R. Wang, Y. Inaguma, T. Yamaguchi, Y.-J. Shan, and T. Nakamura, *ibid.* **82**, 3540 (1999); H. Taniguchi, M. Itoh, and T. Yagi, *ibid.* **99**, 017602 (2007); R. Blinc, B. Zalar, V. V. Laguta, and M. Itoh, *ibid.* **94**, 147601 (2005).
[12] U. T. Höchli, K. Knorr, and A. Loidl, Adv. Phys. **39**, 405 (1990).
[13] A. Chandra, R. Ranjan, D. P. Singh, N. Khare, and D. Pandey, J. Phys.: Condens. Matter **18**, 2977 (2006).
[14] E. Cockayne and B. P. Burton, Phys. Rev. B **62**, 3735 (2000).
[15] W. Kanzig, in *Solid State Physics*, edited by F. Seitz and D. Turnbull (Academic, New York, 1957), Vol. 4.
[16] S. Tripathi, D. Pandey, S. K. Mishra, and P. S. R. Krishna, Phys. Rev. B **77**, 052104 (2008).
[17] J. Rodríguez-Carvajal, Physica B **192**, 55 (1993).
[18] X. Gonze, J.-M. Beuken, R. Caracas, F. Detraux, M. Fuchs, G.-M. Rignanese, L. Sindic, M. Verstraete, G. Zerah, F. Jollet, M. Torrent, A. Roy, M. Mikami, Ph. Ghosez, J.-Y. Raty, and D. C. Allan, Comput. Mater. Sci. **25**, 478 (2002).
[19] L. Bellaiche and David Vanderbilt, Phys. Rev. B **61**, 7877 (2000); N. J. Ramer and A. M. Rappe, J. Phys. Chem. Solids **61**, 315 (2000); L. Bellaiche, Alberto García, and David Vanderbilt, Phys. Rev. Lett. **84**, 5427 (2000); I. A. Kornev, L. Bellaiche, P.-E. Janolin, B. Dkhil, and E. Suard, *ibid.* **97**, 157601 (2006).
[20] B. D. Cullity, *Introduction to Magnetic Materials* (Addison-Wesley Publishing Company Inc., Manila, 1972).
[21] A. M. Glazer, Acta Crystallogr., Sect. B: Struct. Crystallogr. Cryst. Chem. **28**, 3384 (1972); Acta Crystallogr., Sect. A: Cryst. Phys., Diffr., Theor. Gen. Crystallogr. **31**, 756 (1975).
[22] H. T. Stokes, D. M. Hatch, and B. J. Campbell, ISOTROPY, stokes.byu.edu/isotropy.html
[23] See supplementary material at http://link.aps.org/supplemental/10.1103/PhysRevB.81.212101 for Table I and Fig I.
[24] R. J. Hill and H. D. Flack, J. Appl. Crystallogr. **20**, 356 (1987).
[25] R. A. Young, in *The Rietveld Method*, International Union of Crystallography Monographs on Crystallography Vol. 5, edited by R. A. Young (Oxford University Press, New York, 1996), Chap. 1.